Ligand Effects on the Selective Hydrogenation of Nitrobenzene to Cyclohexylamine Using Ruthenium Nanoparticles as Catalysts

M. Rosa Axet, Salvador Conejero, I.C. Gerber

Ligand Effect on the Selective Hydrogenation of Nitrobenzene to Cyclohexylamine using Ruthenium Metal Nanoparticles as Catalyst

M. Rosa Axet,[a*] Salvador Conejero,[b] and Iann C. Gerber [c]

[a] LCC-CNRS, Université de Toulouse, CNRS, 31077 Toulouse, France

[b] Instituto de Investigaciones Químicas (IIQ), Departamento de Química Inorgánica, Centro de Innovación en Química Avanzada (ORFEO-CINCA), CSIC/Universidad de Sevilla, Avenida Américo Vespucio 49, 41092 Sevilla, Spain

[c] LPCNO, Université Fédérale de Toulouse Midi-Pyrénées, INSA-CNRS-UPS, 135 avenue de Rangueil, F-31077 Toulouse, France

rosa.axet@lcc-toulouse.fr

Abstract

A series of ruthenium nanoparticles (Ru NPs) bearing different ligands on their surface have been used as catalysts in the selective hydrogenation of nitrobenzene to cyclohexylamine. Ru-C_{60}, Ru-PVP, Ru-HDA and Ru-IPr, (PVP: polyvinylpyrrolidone; HDA: hexadecylamine, IPr: 1,3-bis(2,6-diisopropylphenyl)imidazol-2-ylidene) have been chosen due to their different electronic properties, HDA and IPr as donor ligands, PVP as polymer with small interaction with the Ru NPs surface and fullerene C_{60} acting as an electron-attractor ligand, while their size and structure remain similar. A clear influence of the ligand on the Ru NPs surface on the catalytic performances was observed. The less donor ligands promote the hydrogenation of the N-phenylhydroxylamine intermediate, which is considered as the rate determining step, leading to the more active catalysts, affecting also the chemoselectivity of the reaction. Density functional theory (DFT) calculations show that the hydride coverage of the Ru NPs plays a key role in the adsorption of N-phenylhydroxylamine on the surface of the NPs. This adsorption is indeed unfavored for realistic coverage values, higher than 1.5H/per surface Ru atom, explaining the accumulation of this intermediate under hydrogenation conditions, as observed with all Ru NPs here studied. In addition, DFT calculations show that the adsorption of N-phenylhydroxylamine is favored when fullerene C_{60} is present on the Ru NPs surface compared to the uncapped Ru NPs, which correlates well with the higher TOF observed for Ru-C_{60} catalysts compared to the other Ru NPs systems bearing more donating ligands, and also the higher selectivity obtained with this catalyst.

Keywords

ruthenium, nanoparticles, ligand effects, catalysis, hydrogenation

Introduction

The effects of coordinated ligands on transition metals in catalysis are well documented.[1-2] Many examples can be found in the literature where the ligand modulates activity and selectivity of the catalytic center, for instance in the hydroformylation[3] or carbonylation of methanol.[4] Although the homogeneous catalytic systems are easier to characterize and therefore to understand and to modulate, their main drawback is that they are not easy to separate from the products making them difficult to reuse and even contaminating the final products. Because of this drawback, most industrial catalytic processes are nowadays based on heterogeneous catalysts. However, in general, heterogeneous catalysts are less selective

and more complicated to characterize and therefore more difficult to understand and tune. In recent years the understanding of heterogeneous catalysts progressed and this emphasized the importance of their precise characterization including the metal-support interactions and the surface chemistry of the metal due to their effect on the catalytic properties.[5-7] The tuning and understanding of the metal-support interaction allows obtaining more selective and efficient heterogeneous catalysts. For instance, a strong electronic metal-support interaction on Pt/CeO_2 catalysts promotes a charge exchange between Pt and CeO_2, increasing the electron density of Pt when compared to other supports (SiO_2, TiO_2 or carbon) as evidenced by Raman and X-ray Photoelectron Spectroscopy (XPS) analyses. This highest electron density on Pt enhances the hydrogen activation at room temperature, leading to more active catalysts in the hydrogenation of quinoline. Also, the easy release of the hydrogenated product, 1,2,3,4-tetrahydroquinoline, prevents the over hydrogenation and improve the selectivity.[8] The chemoselective hydrogenation of halonitroarenes can be enhanced also by modulating the metal-support interaction. Pt NPs supported on several carbon nanotubes (CNT), containing or oxygen functional groups or nitrogen doped, have been prepared. XPS clearly shows a charge transfer from nitrogen species present on the nitrogen doped CNT to Pt NPs, thus generating electron rich Pt NPs in this support. The authors correlate this feature to the highest chemoselectivity of this catalysts when compared with other CNT supports.[9] Cooperation of the support with gold nanoparticles allows obtaining a very selective catalysts for the hydrogenation of nitrostyrene to the corresponding aniline. A preferential adsorption of the reactant on the catalyst through the nitro group in Au/TiO_2 species was found using IR studies and quantum calculations. This preferential adsorption was not observed in gold/silica catalyst, which is not chemoselective for this reaction.[10]

On the other hand, metal nanoparticles (NPs) which to some extent present intermediate characteristics between those of homogeneous and heterogeneous catalysts have been successfully used as catalysts.[11-13] In many cases NPs are stabilized by ligands, limiting their growth -i. e. determining their size and shape-, and keeping them well dispersed -i. e. avoiding their coalescence.[14] These ligands are chemically bonded to the surface of the NPs and can thus affect their catalytic behavior, either by altering the properties of the metal or directly by blocking some of the metal sites. The coordination of ligands to the surface of NPs has been studied in detail for Ru,[15-26] Pt,[27-28] Rh,[29-30] Ir,[25, 31-32] and Au[33-35] NPs mainly with spectroscopic techniques together with Density Functional Theory (DFT) calculations. Even if today the coordination of stabilizing ligands on the surface of NPs is better understood, it is not always the case for the interaction of intermediate catalytic species with the surface of the NPs, and only a few studies are reported.[25, 30, 36-40] The use of those NPs as catalysts has revealed the remarkable effect of the ligands anchored on the surface of the NPs. Pt NPs stabilized with long-chain N-heterocyclic carbenes; used as catalysts in hydroboration reactions clearly show an influence of the bulkiness of the N-substituent of the carbene on the catalytic activity.[41] Also, Pt NPs stabilized with zwitterionic amidinates display a notable ligand effect in the hydrogenation of electron-poor carbonyl groups, where the catalytic activity is influenced by remote groups introduced in the aryl-N-substituents of the amidinates present on the surface of the NPs.[27] Similarly, N-heterocyclic carbene-stabilized Ru NPs are active catalysts in the hydrogenation of aromatic substrates; in this case modulating the activity and the selectivity of this hydrogenation reaction.[22] The surface modification of oleylamine-capped gold NPs with a carbene ligand enhanced the reduction of CO_2 to CO when compared to the unmodified gold NPs. The authors attributed this improvement to the strong σ-donation of the carbene ligand giving electron rich gold surfaces, which could explain the change in the mechanism observed with the carbene modified gold NPs in which a fast electron transfer is detected.[42] Also, the presence of ligands (PhC≡C) in the atomically precise AuAg nanocluster significantly improve the catalytic properties of the cluster compared to the relative bare nanocluster in the oxidation of triethylsilane.[43] Also, the efficiency of RuCo bimetallic nanoparticles in the selective reduction of nitrostyrene to aminostyrene was modulated by the polystyrene support; polymers containing electron-withdrawing substituents consumed faster the substrate.[44] Ultrathin Pt nanowires have been coated with ethylenediamine, which electronic effect shape the catalytic

activity in the hydrogenation of nitrobenzene.[45] The ethylenediamine-capped Pt NPs exhibit a high selectivity to the thermodynamically unfavorable N-phenylhydroxylamine (PHA), while the bare Pt NPs produced the further hydrogenated amine. DFT calculations reveal that the modification of the Pt surface with ethylenediamine makes the Pt electron rich, favoring the adsorption of electron-deficient reactants (nitrobenzene) over electron-rich (PHA) and therefore preventing it to be fully hydrogenated to the aniline.

In a previous study by some of us we described the preparation of a catalysts by decomposition under dihydrogen of (1,5-cyclooctadiene)(1,3,5-cyclooctatriene)ruthenium(0) [Ru(COD)(COT)] in the presence of fullerene C_{60}.[18] The combination of several experimental techniques, together with DFT calculations allowed us to have an insight into the structure of these Ru-C_{60} species. These Ru nanomaterials are composed by Ru-C_{60} polymeric spheres with the surface decorated with Ru NPs. The molecular species self-assembled as spheres consist in a polymeric structure in which a Ru atom is coordinated to two C_{60} displaying a $\eta^{2(6)}$-$\eta^{(6)}$ coordination mode as pointed out by transmission electron microscopy (TEM), Extended X-Ray Absorption Fine Structure (EXAFS), Wide-Angle X-ray Scattering (WAXS), and DFT calculations. Raman and XPS analyses evidenced a charge transfer from Ru to fullerene. These electron-deficient Ru NPs supported on Ru fulleride nanospheres allow the successive and chemoselective hydrogenation of nitrobenzene (NB) to aniline (AN) and then to cyclohexylamine (CA).[39] At first this behavior was attributed to the fact that Ru NPs are electron-deficient, however, DFT calculations have shown that the coordination mode of NB on such nano-objects changes with the hydride coverage of the Ru NPs. At low coverage π-mode coordination is favored, for which both hydrogenation of the aromatic ring and the nitro groups are possible. At high hydride coverage –i.e. hydrogenation reaction conditions-, NO_2-mode coordination prevails, for which only NO_2 hydrogenation is possible. It has been shown that Pt nanoparticles modified with an electron-rich amine can produce very selectively PHA,[45] showing that the electron density of the surface has a large impact in this hydrogenation reaction, in this case, disfavoring the coordination of an intermediate, and leading to a very selective catalyst. The possible ligand effect due to the presence of electron-rich or electron-poor ligand on the Ru NPs surface in the hydrogenation of nitrobenzene to cyclohexylamine has been further investigated in this work. With the purpose, several Ru NPs wearing different ligands on the surface, named Ru-C_{60}, Ru-PVP, Ru-HDA and Ru-IPr (PVP: polyvinylpyrrolidone; HDA: hexadecylamine, IPr: 1,3-bis(2,6-diisopropylphenyl)imidazol-2-ylidene) have been synthesized and used as catalysts in the hydrogenation of nitrobenzene. These previously described Ru NPs, synthesized by the same methodology, have been chosen due to their similar characteristics -size, crystallographic structure, hydride coverage of the surface- while the surface is decorated with ligands which display different electronic properties; HDA and IPr as donor ligands, PVP as polymer with small interaction with the Ru surface and C_{60} acting as an electron-attractor ligand.

Results and discussion

Ruthenium nanoparticles were synthesized by decomposition under dihydrogen of [Ru(COD)(COT)] in the presence of the respective stabilizing compound using previously described (Ru-C_{60},[18] Ru-HDA,[46] Ru-PVP4[46] and Ru-IPr[47]) or modified procedures (Ru-PVP20[46] see experimental section). TEM analyses reveal Ru NPs sizes of 1.6 ± 0.6 nm (Ru-C_{60}), 1.1 ± 0.6 nm (Ru-PVP20), 1.0 ± 0.5 nm (Ru-PVP4), 1.3 ± 0.5 nm (Ru-HDA) and 0.8 ± 0.4 nm (Ru-IPr) (Figure 1). The Ru content being (%): 50.1 (Ru-C_{60}), 19.5 (Ru-PVP20), 4.2 (Ru-PVP4), 41.2 (Ru-HDA) and 30.7 (Ru-IPr).

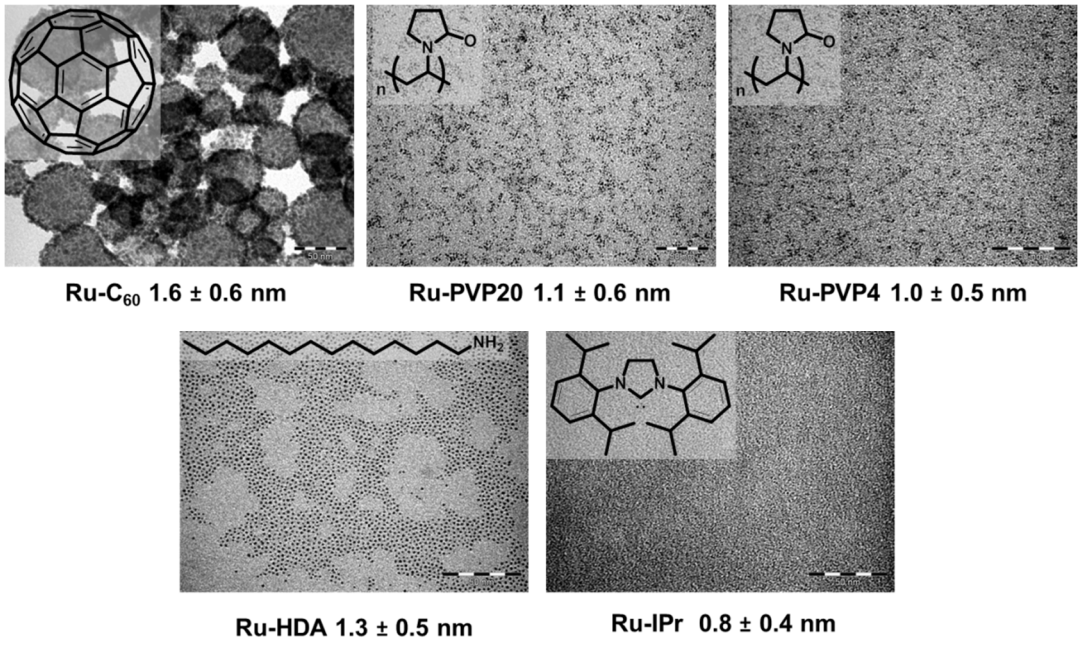

Figure 1. TEM images of Ru-C_{60}, Ru-PVP20, Ru-PVP4, Ru-HDA, and Ru-IPr (scale bar 50 nm).

CO is a vibrational probe to determine the basicity of metal centers, with lower energies of ν_{CO} band indicating more electron density on the metal centers. In order to establish the relative basicity of the Ru NPs here synthesized, CO was added to the solid samples of the Ru NPs and then the Attenuated Total Reflection - Fourier-Transform InfraRed (ATR-FTIR) spectra were recorded (Figure 2 and Figure S2-S6). The ν_{CO} confirmed that Ru-C_{60} are the more electron-deficient Ru NPs showing two bands at 2061 and 1994 cm^{-1}, when compared with the Ru NPs stabilized with PVP which display a ν_{CO} at approximately 2000 cm^{-1}. Ru-IPr and Ru-HDA are the more basic Ru NPs of the series displaying lower frequencies (1982 cm^{-1}; 1918 cm^{-1}, and 1962 cm^{-1}, respectively). By analyzing charge densities out of DFT calculations, on two different molecular models: a pristine Ru_{13} cluster, and a Ru_{13}-$2C_{60}$, supposedly mimicking respectively the electronic structure of Ru-PVP and Ru-C_{60} NPs samples, we confirmed the electron-deficient character of Ru-C_{60} NPs with an averaged electron loss of -0.15e per surface Ru atom when compared to the naked cluster.

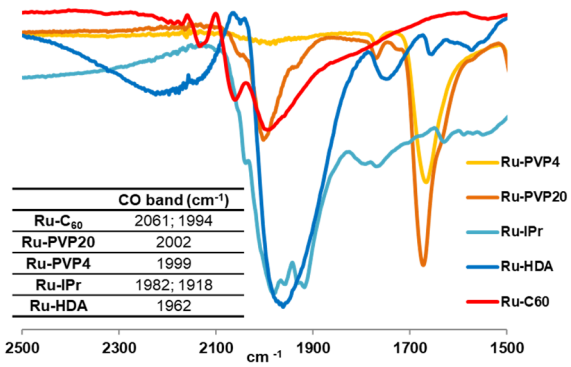

Figure 2. Enlarged portion of the ATR-IR spectra of the Ru nanocatalysts after CO exposure.

Nitrobenzene hydrogenation was studied at 30 bar of H_2 and 80 °C in ethanol (see Table 1). Stepwise hydrogenation first to aniline and then to cyclohexylamine was observed in all cases studied except for Ru-HDA where small amounts of CA were detected at the beginning of the reaction. Ru-C_{60} proceed selectively, first hydrogenating the $-NO_2$ group (Figure 3, purple

curve) to form aniline (Figure 3, green curve), and then after two hours of reaction producing CA (Figure 3, yellow curve) and also dicyclohexylamine (DCA) and N-ethylcyclohexylamine (CA-Et) as byproducts (Figure 3, orange curves). The curves of the other catalysts are presented in the SI (Figure S7-S11).

Table 1. Hydrogenation of Nitrobenzene in Ethanol with Different Ru Catalysts[a]

Catalyst	TOF (h^{-1})[b, c]	Time (h)	Selectivity (%)					
			AN	AN-Et	AN=Et	CA	CA-Et	DCA
Ru-C_{60}	136.9	2	95	4	1	-	-	-
		4	-	-	-	76	10	14
Ru-HDA	129.2	2	76	1	3	16	4	-
		6	-	-	-	83	16	1
Ru-PVP20	82.8	3	82	6	12	-	-	-
		6	-	-	-	63	14	23
Ru-PVP4	71.4	3	76	6	18	-	-	-
		6	-	-	-	63	16	21
Ru-IPr	64.8	3	68	14	18	-	-	-
		6	-	-	-	57	26	17

[a]Reaction conditions: $2.5x10^{-2}$ mmol of Ru, 4 mmol of nitrobenzene, 1 mmol of dodecane (internal standard), 30 bar H_2, 80°C, 30 mL EtOH. [b]Determined by GC-MS using internal standard technique. [c]TOFs calculated at 1 h of reaction related to the % of Ru surface atoms.

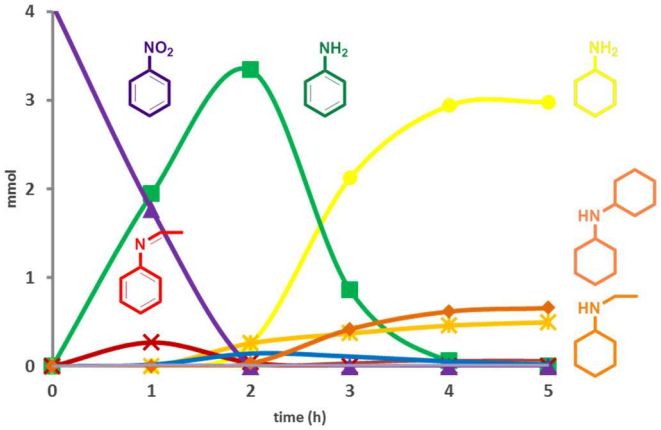

Figure 3. Time-concentration curve for nitrobenzene hydrogenation with Ru-C_{60}. Nitrobenzene (purple curve), aniline (green curve), N-ethylidene-aniline (red curve), cyclohexylamine (yellow curve), dicyclohexylamine (dark orange curve); N-ethylcyclohexylamine (orange curve).

At the beginning of the reaction N-ethylidene-aniline (AN=Et) was also detected in the reaction media (Figure 3, red curve). This intermediate compound was observed in all the nanocatalysts studied, although the detected amount was variable depending on the Ru catalyst used. The lowest quantity was observed for Ru-C_{60} (7%) and Ru-HDA (6%) catalysts, while for the other catalysts N-ethylidene-aniline was detected in the range of 15-20%. It has been proven that Ru can catalyze the reaction of PHA with an alcohol to produce the respective imine.[48] PHA is an intermediate of the nitrobenzene hydrogenation sequence (Scheme 1) and several experimental and theoretical studies point out that the reduction of the N-phenylhydroxylamine is the rate-determining step in the hydrogenation pathway using Au,[49] Pt,[50] Ni[51] or Pd over Pt.[52] In this sense, it seems feasible that AN=Et detected in the reaction media is produced by the reaction of PHA and the ethanol used as the solvent in the presence of Ru, and PHA reacts with the solvent as it is accumulated in the reaction media instead of being hydrogenated. In order to confirm that AN=Et is produced from the reaction of PHA with EtOH, as PHA was never detected in the catalytic solutions, we have performed an NMR tube experiment to follow the reaction of PHA over the Ru nanoparticles. PHA and Ru-IPr were dissolved on THF-d_8 in a screw cap NMR tube. Then, an excess of EtOH was introduced and the NMR tube was heated at 80°C for 1h. The ^{1}H NMR spectrum was recorded showing new signals attributed to the AN=Et, the iminic proton at δ 9.65 ppm as a quartet (J_{HH} = 2.8 Hz) and a doublet (J_{HH} = 2.8

Hz) at δ 2.06 ppm attributed to the methyl group (Figure S12, SI). Also, the ^{1}H NMR spectrum of the brown solution shows that PHA disproportionates to nitrosobenzene, aniline and azoxybenzene. These observations correlate well with the DFT calculations observations (see below), which show that PHA spontaneously disproportionates on the Ru NPs surface to give AN in the absence of hydrides on the surface.

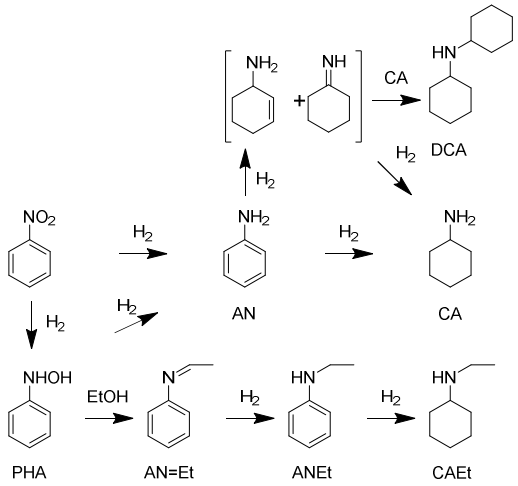

Scheme 1. Simplified reaction pathway for the hydrogenation of nitrobenzene to cyclohexylamine.[7]

As N-ethylidene-aniline is produced from PHA, and taking into account that the hydrogenation of PHA is likely the rate determining step of the reaction, a more important quantity of this compound indicates a less favored hydrogenation, allowing to the reaction of PHA with the solvent. Also, the final amount of CA-Et, which is produced mainly by the hydrogenation of AN=Et (see below, aniline hydrogenation), can be a better indicator of the PHA accumulated during the reaction as it is more stable than AN=Et. Indeed, a good correlation exists between the calculated TOF and the mmol of AN=Et or CA-Et in the analyzed solutions: Ru-C_{60} 136.9 h^{-1}; 0.3 mmol AN=Et; 0.4 mmol CA-Et > Ru-HDA 129.2 h^{-1}; 0.3 mmol AN=Et; 0.6 mmol CA-Et > Ru-PVP20 82.8 h^{-1}; 0.6 mmol AN=Et; 0.5 mmol CA-Et > Ru-PVP4 71.4 h^{-1}; 0.6 mmol AN=Et; 0.6 mmol CA-Et > Ru-IPr 64.8 h^{-1}; 0.7 mmol AN=Et; 1.0 mmol CA-Et. In consequence, also the selectivity of this hydrogenation reaction in EtOH is related to the hydrogenation of PHA. As less favored the reaction is, i. e. increased amount of the AN=Et in the reaction media, the selectivity towards aniline and therefore to cyclohexylamine decreases.

From the analyses of the TOF and the selectivity of the nitrobenzene hydrogenation it can be proposed that the ligand on the Ru nanoparticles surface plays an important role in the catalytic performances of the Ru nanocatalysts. The less basic Ru NPs Ru-C_{60} are the more active and selective in this conditions, while the more basic, Ru-IPr are the less active and selective, the Ru NPs sterically stabilized with the PVP polymer showing intermediate values. The accumulation of the PHA intermediate indicates that basic ligands on the surface of the Ru NPs, as Ru-IPr NPs, disfavor its hydrogenation which is considered the rate determining step, and hence disfavoring the catalytic performances in terms of activity and selectivity. Even if steric effects cannot be completely run out, the stabilizing agents used in this work should minimize this effect: PVP interact very weakly with the metallic surface, HDA is very fluxional,[46] C_{60} is mainly located in the core of the nanospheres,[18] and IPr despite is not fluxional in solution is able to easily accommodate aryl rings on the surface to be hydrogenated indicating that is mobile on the surface.[22, 47] Indeed, Ru-PVP20 and Ru-PVP4 display slightly different TOFs, being Ru-PVP20 the faster of the catalysts as probably the surface is more accessible (less PVP in the sample), indicating a slightly steric effect, but the selectivity seems to be mainly governed by electronic effects as both, Ru-PVP20 and Ru-PVP4, show the same product distribution. The electronic effect on the activity observed here is consequent with the findings

of Zheng et al.;[45] electron rich Pt NPs allow obtaining phenylhydroxylamine very selectively from nitrobenzene. The authors propose, supported by DFT calculations, that the binding of the electron-poor nitrobenzene is favoured while the electron-rich phenylhydroxylamine cannot adsorb easily the electron-rich surface. To get better insights of the interaction of PHA molecules with Ru-NPs, we have performed DFT calculations on four different Ru NPs models: a naked Ru_{13}, a hydrogenated Ru_{13} with a coverage values of 1.5H/per surface Ru atom ($Ru_{13}H_{18}$), a Ru_{13}-$(C_{60})_2$ complex and a hydrogenated $Ru_{13}H_{18}$-$(C_{60})_2$ one; hydrogenated Ru NPs models simulating the surface of the NPs under hydrogenation conditions.[28] Adsorption energies of a single PHA molecule on those models are given in Table 2, after a careful checking of the nature of the most stable geometries. We have also considered the effect of solvent, but using an implicit solvent model procedure, see the computational details below. When the Ru NPs are not covered by any hydrides, the PHA molecule spontaneously dissociates to form AN while the remaining O atom lies on the surface in a Top position with a Ru-O distance of 1.68 Å. As it can be seen in Figure 4 panel a), the AN molecule presents a π-mode coordination with the aromatic cycle interacting with three Ru atoms. The coordination mode is 2 C-C bonds over a Ru atom and one C on top position. The thermodynamics balance in those two cases are clearly unfavorable (<-120 kcal/mol) for the stability of PHA in the presence of non-hydrogenated Ru NPs. However, as we pointed out recently, the influence of hydrides is crucial, as soon as a threshold values of more than 1 H per surface Ru atom is yielded, since coordination modes stability can be inverted.[39] Here the effects of hydride coverage are of two types: first they take electronic densities from Ru atoms, as given in Table 2, and secondly their presence on the surface stabilizes PHA molecules since the hydroxyl group does not interact with any Ru atom. As a consequence, the adsorption energies are much smaller: being -10 and -30 kcal/mol for the Ru-PVP and Ru-C_{60} nanocatalyst models, respectively. In order to confirm that PHA disproportionates on the Ru NPs surface in the absence of hydrides on the surface the following experiment was set up: PHA was dissolved in EtOH and then Ru-IPr was added to the solution, then the dark brown dispersion was heated at 80°C in a Fisher Porter bottle under argon, and the evolution of the reaction was followed by GC. The GC analysis of the solution at time zero indicates that PHA disproportionates already at room temperature to form 30% of nitrosobenzene, 40% of aniline and 20% of azoxybenzene, probably formed by the condensation of PHA and nitrosobenzene, remaining 10% of the initial PHA in the solution. After 40 min heating at 80°C the reaction evolved to the formation of azoxybenzene (66%) remaining 33% of aniline and 1% of nitrosobenzene. The solution was keep at this temperature overnight, the GC analysis of the solution showing no longer evolution (70% of azoxybenzene and 30% of aniline).

Table 2. Adsorption energy of PHA on different Ru_{13} NPs

Initial State	Final State	E_{ads} in vacuum (kcal/mol)	E_{ads} in EtOH (kcal/mol)	Averaged electronic loss per Surface Ru atoms[a]
Ru_{13} + PHA	$Ru_{13}O$ + AN	-140	-145	-0.09
$Ru_{13}H_{18}$ + PHA	$Ru_{13}H_{18}$ + PHA	-10	-9	-0.35
Ru_{13}-$(C_{60})_2$ + PHA	$Ru_{13}O$-$(C_{60})_2$ + AN	-122	-126	-0.19
$Ru_{13}H_{18}$-$(C_{60})_2$+ PHA	$Ru_{13}H_{18}$-$(C_{60})_2$ + PHA	-30	-32	-0.33

[a]In comparison with a naked Ru_{13} NP

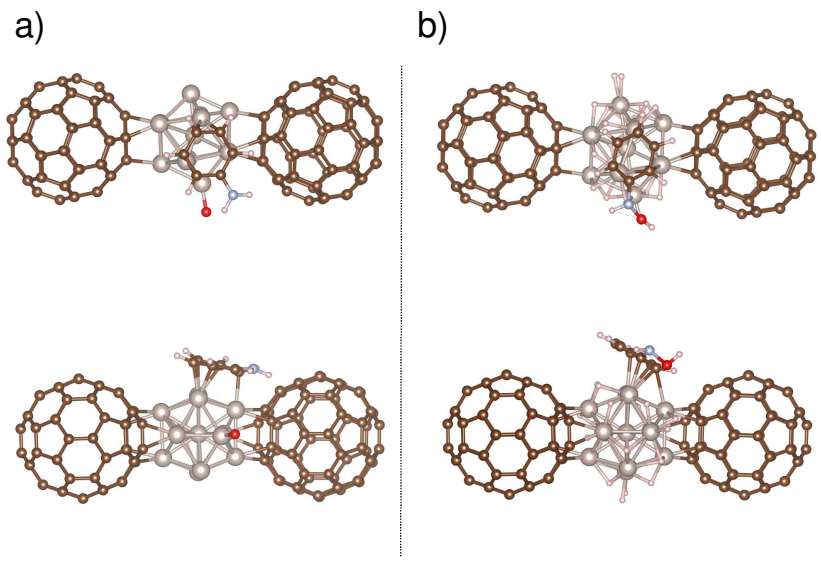

Figure 4. Most stable states after PHA adsorption on (a) Ru_{13}-$(C_{60})_2$ and (b) $Ru_{13}H_{18}$-$(C_{60})_2$.

On the other hand, Ru-HDA showed a different trend when compared to the other catalyst here studied. The reaction was not as chemoselective as observed for the other nanocatalyst since small amounts of cyclohexylamine (less than 10%) were detected after 1h of reaction, while nitrobenzene was still present in the reaction media. This different behavior can also affect the TOF and the selectivity considering that a basic molecule, CA, is present in the reaction media, being not comparable with the rest of the nanocatalyst. To clarify the role of CA two sets of experiments were carried out using Ru-IPr nanocatalysts, which provides the highest quantities of AN=Et and is the slowest catalyst, adding 0.5 or 1.5 mmol of CA in the reaction media. The first analysis of the data shows that the TOFs of the NB hydrogenation are higher when adding CA (Table 3, 64.8 h^{-1} to 91.4 h^{-1} (0.5 mmol of CA) and 138.3 h^{-1} (1.5 mmol of CA)); and the AN=Et detected in the reaction media decreases (0.7 mmol AN=Et for Ru-IPr; 0.4 mmol AN=Et for Ru-IPr + 0.5 mmol of CA; and 0.2 mmol AN=Et for Ru-IPr + 1.5 mmol of CA). Also, the concentration curves show that the CA introduced at the beginning of the reaction was completely consumed in the Ru-IPr + 0.5 mmol of CA test whereas 60% of the initial CA was reacted in the Ru-IPr + 1.5 mmol of CA experiment. It seems reasonable to propose that the PHA interacts with the strongly basic CA favoring the hydrogenation rate-determining step. However, we cannot rule out the possibility that this interaction takes place directly with nitrobenzene. It has been previously proposed that NB can interact with amino groups to form intermediary species (hydrogen bonded NB-AN adducts) which promoted the NB hydrogenation rate.[53] Indeed, during the Ru-IPr + 1.5 mmol of CA experiment an intermediate species has been detected that, according to the mass and ^{1}H NMR spectra (see SI), corresponds to the imine produced by reaction of CA and EtOH, CA=Et. However, in the Ru-IPr + 0.5 mmol of CA experiment the double alkylation product with EtOH ($CA(Et)_2$) was identified. The consumption of the initial CA in the Ru-IPr + 1.5 mmol of CA experiment corresponds to 0.8 mmol, which is a similar value than the AN=Et produced during the catalysis performed without CA, pointing out that probably CA is more likely interacting with PHA than with NB. The double alkylation product $CA(Et)_2$ found in the Ru-IPr + 0.5 mmol of CA experiment is due to the lack of enough CA to react so CA-Et, also a strong base, reacts in turn with the PHA present in the reaction media. Furthermore, these results can explain the higher hydrogenation rate observed for Ru-HDA. HDA is a ligand which binds reversibly to the surface of metal nanoparticles, i. e. free and coordinated amine are present in the solution.[28, 46] As HDA is also a strong base (the pKa of HDA and CA is 10.6) which can enhance, as CA, the hydrogenation reaction of NB, it could explain the different behavior in terms of activity and selectivity when compared with the other catalysts used here.

Table 3. Hydrogenation of Nitrobenzene in Ethanol with Ru-IPr Catalysts[a]

Catalyst	TOF (h^{-1})[b, c]	Time (h)	Selectivity (%)							
			AN	AN-Et	AN=Et	CA	CA-Et	DCA	CA-$(Et)_2$	CA=Et
Ru-IPr	64.8	3	68	14	18	-	-	-	-	-
		6	-	-	-	57	26	17	17	-
Ru-IPr + CA (0.5mmol)	91.4	2	66	6	9	-	12	-	7	-
			-	-	-	52	23	15	10	-
Ru-IPr + CA (1.5mmol)	138.3	1	54	1	5	12	8	-	-	20
			-	-	-	55	32	12	1	-

[a]Reaction conditions: $2.5x10^{-2}$ mmol of Ru, 4 mmol of nitrobenzene, 1 mmol of dodecane (internal standard), 30 bar H_2, 80°C, 30 mL EtOH. [b]Determined by GC-MS using internal standard technique. [c]TOFs calculated at 1 h of reaction related to the % of Ru surface atoms.

Table 4. Hydrogenation of Aniline in Ethanol with Different Ru Catalysts[a]

Catalyst	TOF (h^{-1})[b, c]	Time (h)	Selectivity (%)		
			CA	CAEt	DCA
Ru-IPr	170.9	1	97	2	1
Ru-HDA	149.4	3	96	0	4
Ru-C_{60}	236.1	1	87	1	12
Ru-PVP4	207.0	1	84	3	13
Ru-PVP20	170.1	2	81	0	19

[a]Reaction conditions: $2.5x10^{-2}$ mmol of Ru, 4 mmol of aniline, 1 mmol of dodecane (internal standard), 30 bar H_2, 80°C, 30 mL EtOH. [b]Determined by GC-MS using internal standard technique. [c]TOFs calculated a 1 h of reaction related to the % of Ru surface atoms.

The hydrogenation of aniline was studied using the same reaction conditions as used for the nitrobenzene hydrogenation (30 bar of H_2 and 80 °C in ethanol) in order to establish if the presence of CA-Et is due to the hydrogenation of AN=Et or if it is also formed from CA (Table 4). The selectivity was high in all cases, up to 97% of CA using Ru-IPr as catalysts, because the formation of CA-Et is almost suppressed. This indicates that the CA-Et byproduct is mainly produced by the hydrogenation of the imine intermediate AN=Et, formed during the nitrobenzene hydrogenation. The calculated TOFs follow the next trend: Ru-C_{60} > Ru-PVP4 > Ru-PVP20 = Ru-IPr > Ru-HDA; and the selectivity was highly dependent on the Ru NPs used. The more basic ligands on the Ru NPs surface give better selectivity towards CA, as dicyclohexylamine is not produced. This byproduct is produced by the condensation of the cyclohexylamine with one partially hydrogenated intermediate (see Scheme 1).[54] It has been observed that acidic medium leads to less selective hydrogenation of aniline to produce cyclohexylamine,[55] probably as a consequence of both activation of the imine intermediate and the quenching of the ammonia by the presence of the acid.[56] This would explain why Ru NPs bearing more basic ligands do not promote this acid catalyzed reaction increasing the selectivity towards CA. In addition, the CA selectivity obtained with Ru-IPr and Ru-HDA (97% and 96%, respectively) is one of the highest reported to our knowledge.[53, 57-58] The high selectivity of the Ru-IPr in the hydrogenation of AN (Table 4) is in contrast with the selectivity observed in the total hydrogenation of NB (Table 1). The relative percentage of CA/DCA obtained in the NB hydrogenation (Table 1) is: Ru-C_{60}: 84%CA; 16%DCA; Ru-HDA: 99%CA; 1%DCA; Ru-PVP20: 73%CA; 27%DCA; Ru-PVP4: 75%CA; 25%DCA; Ru-IPr: 77%CA; 23%DCA. Ru-C_{60} and Ru-HDA present a relative percentage very close to that observed in the direct hydrogenation of aniline (Table 4), in contrast Ru-IPr (and also Ru-PVP systems), produces more DCA in the stepwise hydrogenation of NB. These data suggest that PHA (and/or another intermediate formed during the -NO_2 group reduction) which is more accumulated when using Ru-PVP and Ru-IPr catalysts could favour the formation of DCA. In order to clarify this point the hydrogenation of AN was studied by adding PHA in the reaction media. Ru-IPr was used as catalysts and the presence of PHA (1 mmol) lead to a less selective reaction (91% of CA; 2% CA-Et; 7% DCA) pointing out that the PHA can promote the condensation of CA and the partially hydrogenated AN.

Conclusions

The stepwise selective hydrogenation of nitrobenzene to aniline and then to cyclohexylamine has been observed for the Ru catalysts: Ru-C_{60}, Ru-PVP, and Ru-IPr. Ru-HDA exhibits a slightly different behavior as cyclohexylamine was detected on the reaction media when nitrobenzene was not completely consumed. These results point out that the stepwise hydrogenation is modulate by another parameter. In a previous study by some of us[39] DFT calculations showed that is the hydride coverage of the Ru NPs which is key to modulate the coordination mode of the substrates. Here, DFT calculations clearly show that the adsorption of the N-phenylhydroxylamine, which its hydrogenation is considered as the rate determining step of this multistep hydrogenation, on the Ru NPs surface depends strongly on the hydride coverage. Indeed, PHA disproportionates on Ru_{13} and Ru_{13}-$(C_{60})_2$ to give aniline, behaviour observed experimentally in this work, but also described elsewhere.[59] PHA adsorbs weakly on the surface of hydrogenated Ru NPs ($Ru_{13}H_{18}$ and $Ru_{13}H_{18}$-$(C_{60})_2$). The weak interaction of PHA with the Ru surface can explain why PHA is accumulated on the reaction media (in this study correlated to the N-ethylidene-aniline detected on all the reaction media studied), leading to the stepwise hydrogenation. Indeed, we have probed here that when adding a strong base (CA) in the hydrogenation solution, the TOFs increased; also explaining why Ru-HDA is much more active than expected as HDA is likely acting not only as stabilizing ligand but also as a strong base. Although the hydride coverage seems to be crucial for the adsorption of the PHA intermediate, the ligands on the surface of the Ru NPs modulate the activity and selectivity of the nitrobenzene hydrogenation reaction. Ru-C_{60} showed the better performances in terms of activity and selectivity (TOF= 136.9 h^{-1}; 95% AN) as probably promotes better the hydrogenation of PHA. DFT calculations show that the coordination of fullerene C_{60} on the surface of the NPs allows a stronger coordination of the PHA when compared to bare Ru NPs, fitting well with the experimental results. In contrast, Ru-IPr is less active and selective, however, this performance can be explored in the future in order to obtain selectively N-hydroxylanilines which are industrially important intermediates.[60-63] A ligand effect was also observed in the aniline hydrogenation, the basic stabilizers IPr and HDA leading to high selectivities to CA (97% and 96%, respectively).

Experimental part

General Methods

All operations were carried out under argon atmosphere using standard Schlenk techniques or in an MBraun glovebox. Solvents were purified by standard methods or by an MBraun SPS-800 solvent purification system. [Ru(COD)(COT)] was purchased from Nanomeps Toulouse, fullerene C_{60}, HDA, PVP, nitrobenzene, aniline, cyclohexylamine and dodecane from Sigma-Aldrich, CO and H_2 from Air Liquid. All these reactants were used as received. IPr was synthesised following the procedure described elsewhere.[64]

The ruthenium content was established by inductively coupled plasma optical emission spectroscopy (ICP-OES) performed at the LCC in a Thermo Scientific ICAP 6300 instrument.

Liquid NMR were performed on a Bruker Avance 300 instrument.

ATR-IR spectra were recorded on a Perkin-Elmer GX2000 spectrometer available in a glovebox, in the range 4000-400 cm^{-1}.

TEM and HRTEM analyses were performed at the “Centre de microcaracterisation Raimond Castaing, UMS 3623, Toulouse”. TEM by using a JEOL JEM 1011 CX-T electron microscope operating at 100 kV with a point resolution of 4.5 Å. The approximation of the particles mean

size was made through a manual analysis of enlarged micrographs by measuring at least 200 particles on a given grid.

GC analyses were performed on a Perkin Elmer Autosystem XL equipped with a Restek Rtx 5-Amine column (30 m, 0.53 mm, 1 µm). GC-MS analyses were performed in a PerkinElmer Autosystem GC equipped with an Elite-5MS Capillary Column (30 m × 0.25 mm × 0.25 µm) coupled to a Turbo Mass mass spectrometer. Quantitative analyses of the reaction mixtures were performed via GC techniques using calibration solutions of commercially available products.

DFT calculations were carried out using the Vienna *ab initio* simulation package VASP.[65-68] The code uses the full-potential projector augmented wave (PAW) framework.[69-70] Exchange-correlation effects have been approximated using the PBE functional[71] and applied in spin-polarized calculations. A kinetic-energy cutoff of 400 eV was found to be sufficient to achieve a total-energy convergence within several meV, considering a Gamma only k-point sampling calculations for all the considered complexes, in conjunction with a gaussian smearing of 0.05 eV. During geometry optimization runs and cell relaxations, all the atoms were fully relaxed until forces on individual atoms were smaller than 0.01 eV/Å. Calculation cells for isolated molecules and complexes were 25x26x27 $Å^3$, to avoid spurious interactions between periodic images. Figures of the different geometries were produced thanks to the 3D visualization program VESTA.[72] Henkelman's software[73] was used to performed Bader charge analysis.
Implicit solvent model has been included in the calculations as proposed by Hennig et al.[74-75] The optimal geometries upon Hydrogen adsorption were constructed following the results of Ref[76], meaning that all available μ_3 sites were occupied and then the top sites and if necessary some Bridge sites were used to build the starting geometries, before PHA adsorption. The interaction of an EtOH molecule and the different Ru NPs models has been investigated and provide similar adsorption modes and thus adsorption energies as compared to PHA.

Synthesis of Ru nanoparticles

In a typical experiment [Ru(COD)(COT)] complex was introduced in a Fisher-Porter bottle, and a solution of the desired stabilizer was then introduced in the reactor. The resulting solution was pressurized with 3 bar of H_2. The solution, which turned black after few minutes of reaction, was kept under stirring overnight at room temperature. After this period of time, excess of H_2 was eliminated and the volume of solvent was reduced under vacuum. Pentane was then added to the colloidal suspension to precipitate the Ru nanoparticles. After filtration under argon with a cannula, the black solid powder was washed twice with pentane and filtrated again before drying under vacuum. For each ratio studied, the quantities of reactants are detailed hereafter.

Ru-C_{60}: 250 mg (0.79 mmol) of [Ru(COD)(COT)]; 28.5 mg (0.04 mmol) of fullerene C_{60} and 125 mL of CH_2Cl_2. Yield: 105 mg. ICP analysis Ru: 50.1%

Ru-HDA: 250 mg (0.79 mmol) of [Ru(COD)(COT)]; 43 mg (0.18 mmol) of HDA and 160 mL of THF. Yield: 125 mg. ICP analysis Ru: 41.1%

Ru-PVP4 5/1: 150 mg (0.48 mmol) of [Ru(COD)(COT)]; 1000 mg of PVP and 60 mL of THF. Yield: 800 mg. ICP analysis Ru: 4.2%

Ru-PVP20: 90 mg (0.29 mmol) of [Ru(COD)(COT)]; 100 mg of PVP and 40 mL of THF. Yield: 80 mg. ICP analysis Ru: 19.5%

Ru-IPr: 240 mg (0.76 mmol) of [Ru(COD)(COT)]; 148 mg (0.38 mmol) of IPr and 90 mL of pentane. Yield: 164 mg. ICP analysis Ru: 30.7%

Surface reactivity with CO

The adsorption of carbon monoxide on the surface of the nanostructures was performed in the solid state as follows. A purified sample of nanoparticles was introduced in a Fischer-Porter bottle. The reactor was pressurized with 1.5 bar of CO for 24 h. Then, the CO gas was evacuated under vacuum for 20 min and the ATR-IR spectra were recorded.

General procedure for the hydrogenation of nitrobenzene and aniline

Hydrogenation reactions were performed in Top Industry high pressure and temperature Stainless steel autoclave with a controlling system. In a typical experiment, the autoclave was purged by three vacuum/argon cycles. The mixture of the Ru catalysts, dodecane (as internal standard, 1 mmol) and the corresponding substrate (4 mmol) in 30 mL of ethanol was prepared in a glovebox, ultrasonicated for 5 min and then transferred into a high-pressure autoclave under argon atmosphere. The autoclave was heated to 80°C and pressurized with a constant pressure of 30 bar of H_2; the stirring rate was fixed at 1000 rpm. Samples of the reaction mixture were taken periodically and then analysed by GC and/or GC-MS.

Supporting Information

The Supporting Information is available free of charge at http://pubs.acs.org.

TEM images of Ru nanoparticles together with their respective size histogram, ATR-IR spectrum of Ru NPs, calculation of fraction of surface atoms, time-concentration curves for nitrobenzene hydrogenation with Ru nanoparticles, mean particle size of the Ru NPs before and after catalysis, NMR spectrum of the reaction of N-phenylhydroxylamine with ethanol in the presence of Ru-IPr, GC-MS of the reaction mixture Ru-IPr + CA at 1h of reaction, NMR spectrum of the reaction mixture Ru-IPr + CA at 1h of reaction (PDF).

Acknowledgements

This work was supported by the Centre National de la Recherche Scientifique (CNRS), which we gratefully acknowledge. Financial support (FEDER contribution) from the MINECO (Projects CTQ2016-76267-P and CTQ2016-81797-REDC). I.C.G. acknowledges the Calcul en Midi-Pyrénées initiative CALMIP (Project p0812) for allocations of computer time. This work was also granted access to the HPC resources of CINES and IDRIS under the allocation 2017-A0040906649 made by GENCI.

References

1. Gillespie, J. A.; Zuidema, E.; van Leeuwen, P. W. N. M.; Kamer, P. C. J., *Phosphorus Ligand Effects in Homogeneous Catalysis and Rational Catalyst Design*. John Wiley & Sons Ltd.: 2012; p 1-26.
2. van Leeuwen, P. W. N. M., *Homogeneous Catalysis: Understanding the Art*. Springer: 2004; p 424 pp.
3. van Leeuwen, P. W. N. M.; Claver, C.; Editors, *Rhodium Catalyzed Hydroformylation. [In: Catal. Met. Complexes, 2000; 22]*. Kluwer: 2000; p 284 pp.
4. Thomas, C. M.; Suss-Fink, G., Ligand effects in the rhodium-catalyzed carbonylation of methanol. *Coord. Chem. Rev.* **2003,** 243, 125-142. 10.1016/s0010-8545(03)00051-1.
5. Navalon, S.; Dhakshinamoorthy, A.; Alvaro, M.; Garcia, H., Metal nanoparticles supported on two-dimensional graphenes as heterogeneous catalysts. *Coord. Chem. Rev.* **2016,** 312, 99-148. 10.1016/j.ccr.2015.12.005.
6. Schauermann, S.; Nilius, N.; Shaikhutdinov, S.; Freund, H.-J., Nanoparticles for Heterogeneous Catalysis: New Mechanistic Insights. *Acc. Chem. Res.* **2013,** 46, 1673-1681. 10.1021/ar300225s.
7. Song, J.; Huang, Z.-F.; Pan, L.; Li, K.; Zhang, X.; Wang, L.; Zou, J.-J., Review on selective hydrogenation of nitroarene by catalytic, photocatalytic and electrocatalytic reactions. *Appl. Catal., B* **2018,** 227, 386-408. 10.1016/j.apcatb.2018.01.052.

8. Zhang, S.; Xia, Z.; Ni, T.; Zhang, Z.; Ma, Y.; Qu, Y., Strong electronic metal-support interaction of Pt/CeO_2 enables efficient and selective hydrogenation of quinolines at room temperature. *J. Catal.* **2018,** 359, 101-111. 10.1016/j.jcat.2018.01.004.
9. Shi, W.; Zhang, B.; Lin, Y.; Wang, Q.; Zhang, Q.; Su, D. S., Enhanced Chemoselective Hydrogenation through Tuning the Interaction between Pt Nanoparticles and Carbon Supports: Insights from Identical Location Transmission Electron Microscopy and X-ray Photoelectron Spectroscopy. *ACS Catal.* **2016,** 6, 7844-7854. 10.1021/acscatal.6b02207.
10. Boronat, M.; Concepcion, P.; Corma, A.; Gonzalez, S.; Illas, F.; Serna, P., A Molecular Mechanism for the Chemoselective Hydrogenation of Substituted Nitroaromatics with Nanoparticles of Gold on TiO2 Catalysts: A Cooperative Effect between Gold and the Support. *J. Am. Chem. Soc.* **2007,** 129, 16230-16237. 10.1021/ja076721g.
11. Astruc, D.; Editor, *Nanoparticles and Catalysis*. Wiley-VCH Verlag GmbH & Co. KGaA: 2008; p 640 pp.
12. Suib, S. L.; Editor, *New and Future Developments in Catalysis: Catalysis by Nanoparticles*. Elsevier B.V.: 2013; p 499 pp.
13. Philippot, K.; Lignier, P.; Chaudret, B., Organometallic Ruthenium Nanoparticles and Catalysis. *Top. Organomet. Chem.* **2015,** 48, 319-370. 10.1007/3418_2014_83.
14. Amiens, C.; Ciuculescu-Pradines, D.; Philippot, K., Controlled metal nanostructures: Fertile ground for coordination chemists. *Coord. Chem. Rev.* **2016,** 308, 409-432. 10.1016/j.ccr.2015.07.013.
15. Novio, F.; Monahan, D.; Coppel, Y.; Antorrena, G.; Lecante, P.; Philippot, K.; Chaudret, B., Surface Chemistry on Small Ruthenium Nanoparticles: Evidence for Site Selective Reactions and Influence of Ligands. *Chem. - Eur. J.* **2014,** 20, 1287-1297. 10.1002/chem.201303935.
16. Ganji, P.; van Leeuwen, P. W. N. M., Phosphine Supported Ruthenium Nanoparticle Catalyzed Synthesis of Substituted Pyrazines and Imidazoles from α-Diketones. *J. Org. Chem.* **2017,** 82, 1768-1774. 10.1021/acs.joc.6b03032.
17. Leng, F.; Gerber, I. C.; Lecante, P.; Bentaleb, A.; Munoz, A.; Illescas, B. M.; Martin, N.; Melinte, G.; Ersen, O.; Martinez, H.; Axet, M. R.; Serp, P., Hexakis [60]Fullerene Adduct-Mediated Covalent Assembly of Ruthenium Nanoparticles and Their Catalytic Properties. *Chem. - Eur. J.* **2017,** 23, 13379-13386. 10.1002/chem.201701043.
18. Leng, F.; Gerber, I. C.; Lecante, P.; Bacsa, W.; Miller, J.; Gallagher, J. R.; Moldovan, S.; Girleanu, M.; Axet, M. R.; Serp, P., Synthesis and structure of ruthenium-fullerides. *RSC Adv.* **2016,** 6, 69135-69148. 10.1039/c6ra12023g.
19. Gutmann, T.; Walaszek, B.; Xu, Y.; Waechtler, M.; del Rosal, I.; Gruenberg, A.; Poteau, R.; Axet, R.; Lavigne, G.; Chaudret, B.; Limbach, H.-H.; Buntkowsky, G., Hydrido-Ruthenium Cluster Complexes as Models for Reactive Surface Hydrogen Species of Ruthenium Nanoparticles. Solid-State 2H NMR and Quantum Chemical Calculations. *J. Am. Chem. Soc.* **2010,** 132, 11759-11767. 10.1021/ja104229a.
20. Garcia-Anton, J.; Axet, M. R.; Jansat, S.; Philippot, K.; Chaudret, B.; Pery, T.; Buntkowsky, G.; Limbach, H.-H., Reactions of olefins with ruthenium hydride nanoparticles: NMR characterization, hydride titration, and room-temperature C-C bond activation. *Angew. Chem., Int. Ed.* **2008,** 47, 2074-2078. 10.1002/anie.200704763.
21. Gual, A.; Axet, M. R.; Philippot, K.; Chaudret, B.; Denicourt-Nowicki, A.; Roucoux, A.; Castillon, S.; Claver, C., Diphosphite ligands derived from carbohydrates as stabilizers for ruthenium nanoparticles: promising catalytic systems in arene hydrogenation. *Chem. Commun.* **2008**, 2759-2761. 10.1039/b802316f.
22. Gonzalez-Galvez, D.; Lara, P.; Rivada-Wheelaghan, O.; Conejero, S.; Chaudret, B.; Philippot, K.; van Leeuwen, P. W. N. M., NHC-stabilized ruthenium nanoparticles as new catalysts for the hydrogenation of aromatics. *Catal. Sci. Technol.* **2013,** 3, 99-105. 10.1039/c2cy20561k.
23. Tschan, M. J. L.; Diebolt, O.; van Leeuwen, P. W. N. M., Ruthenium Metal Nanoparticles in Hydrogenation: Influence of Phosphorus-Ligands. *Top. Catal.* **2014,** 57, 1054-1065. 10.1007/s11244-014-0270-z.
24. Gonzalez-Galvez, D.; Nolis, P.; Philippot, K.; Chaudret, B.; van Leeuwen, P. W. N. M., Phosphine-Stabilized Ruthenium Nanoparticles: The Effect of the Nature of the Ligand in Catalysis. *ACS Catal.* **2012,** 2, 317-321. 10.1021/cs200633k.
25. Cano, I.; Martinez-Prieto, L. M.; Fazzini, P. F.; Coppel, Y.; Chaudret, B.; van Leeuwen, P. W. N. M., Characterization of secondary phosphine oxide ligands on the surface of iridium nanoparticles. *Phys. Chem. Chem. Phys.* **2017,** 19, 21655-21662. 10.1039/c7cp03439c.
26. Salas, G.; Campbell, P. S.; Santini, C. C.; Philippot, K.; Costa Gomes, M. F.; Padua, A. A. H., Ligand effect on the catalytic activity of ruthenium nanoparticles in ionic liquids. *Dalton Trans.* **2012,** 41, 13919-13926. 10.1039/c2dt31644g.
27. Martinez-Prieto, L. M.; Cano, I.; Marquez, A.; Baquero, E. A.; Tricard, S.; Cusinato, L.; del Rosal, I.; Poteau, R.; Coppel, Y.; Philippot, K.; Chaudret, B.; Campora, J.; van Leeuwen, P. W. N. M., Zwitterionic amidinates as effective ligands for platinum nanoparticle hydrogenation catalysts. *Chem. Sci.* **2017,** 8, 2931-2941. 10.1039/c6sc05551f.
28. Martinez-Prieto, L. M.; Chaudret, B., Organometallic Ruthenium Nanoparticles: Synthesis, Surface Chemistry, and Insights into Ligand Coordination. *Acc. Chem. Res.* **2018,** 51, 376-384. 10.1021/acs.accounts.7b00378.
29. Martinez-Espinar, F.; Blondeau, P.; Nolis, P.; Chaudret, B.; Claver, C.; Castillon, S.; Godard, C., NHC-stabilised Rh nanoparticles: Surface study and application in the catalytic hydrogenation of aromatic substrates. *J. Catal.* **2017,** 354, 113-127. 10.1016/j.jcat.2017.08.010.
30. Axet, M. R.; Castillon, S.; Claver, C.; Philippot, K.; Lecante, P.; Chaudret, B., Chiral diphosphite-modified rhodium(0) nanoparticles: catalyst reservoir for styrene hydroformylation. *Eur. J. Inorg. Chem.* **2008**, 3460-3466. 10.1002/ejic.200800421.

31. Cano, I.; Martinez-Prieto, L. M.; Chaudret, B.; van Leeuwen, P. W. N. M., Iridium versus Iridium: Nanocluster and Monometallic Catalysts Carrying the Same Ligand Behave Differently. *Chem. - Eur. J.* **2017,** 23, 1444-1450. 10.1002/chem.201605352.
32. Cano, I.; Tschan, M. J. L.; Martinez-Prieto, L. M.; Philippot, K.; Chaudret, B.; van Leeuwen, P. W. N. M., Enantioselective hydrogenation of ketones by iridium nanoparticles ligated with chiral secondary phosphine oxides. *Catal. Sci. Technol.* **2016,** 6, 3758-3766. 10.1039/c5cy02206a.
33. Haekkinen, H., The gold-sulfur interface at the nanoscale. *Nat. Chem.* **2012,** 4, 443-455. 10.1038/nchem.1352.
34. Cano, I.; Huertos, M. A.; Chapman, A. M.; Buntkowsky, G.; Gutmann, T.; Groszewicz, P. B.; van Leeuwen, P. W. N. M., Air-Stable Gold Nanoparticles Ligated by Secondary Phosphine Oxides as Catalyst for the Chemoselective Hydrogenation of Substituted Aldehydes: a Remarkable Ligand Effect. *J. Am. Chem. Soc.* **2015,** 137, 7718-7727. 10.1021/jacs.5b02802.
35. Cano, I.; Chapman, A. M.; Urakawa, A.; van Leeuwen, P. W. N. M., Air-Stable Gold Nanoparticles Ligated by Secondary Phosphine Oxides for the Chemoselective Hydrogenation of Aldehydes: Crucial Role of the Ligand. *J. Am. Chem. Soc.* **2014,** 136, 2520-2528. 10.1021/ja411202h.
36. Foppa, L.; Coperet, C.; Comas-Vives, A., Increased Back-Bonding Explains Step-Edge Reactivity and Particle Size Effect for CO Activation on Ru Nanoparticles. *J. Am. Chem. Soc.* **2016,** 138, 16655-16668. 10.1021/jacs.6b08697.
37. Cusinato, L.; Martinez-Prieto, L. M.; Chaudret, B.; del Rosal, I.; Poteau, R., Theoretical characterization of the surface composition of ruthenium nanoparticles in equilibrium with syngas. *Nanoscale* **2016,** 8, 10974-10992. 10.1039/c6nr01191h.
38. Almora-Barrios, N.; Cano, I.; van Leeuwen, P. W. N. M.; Lopez, N., Concerted Chemoselective Hydrogenation of Acrolein on Secondary Phosphine Oxide Decorated Gold Nanoparticles. *ACS Catal.* **2017,** 7, 3949-3954. 10.1021/acscatal.7b00355.
39. Leng, F.; Gerber, I. C.; Lecante, P.; Moldovan, S.; Girleanu, M.; Axet, M. R.; Serp, P., Controlled and Chemoselective Hydrogenation of Nitrobenzene over Ru@C60 Catalysts. *ACS Catal.* **2016,** 6, 6018-6024. 10.1021/acscatal.6b01429.
40. Soule, J.-F.; Miyamura, H.; Kobayashi, S., Copolymer-Incarcerated Nickel Nanoparticles with N-Heterocyclic Carbene Precursors as Active Cross-Linking Agents for Corriu-Kumada-Tamao Reaction. *J. Am. Chem. Soc.* **2013,** 135, 10602-10605. 10.1021/ja404006w.
41. Martinez-Prieto, L. M.; Rakers, L.; Lopez-Vinasco, A. M.; Cano, I.; Coppel, Y.; Philippot, K.; Glorius, F.; Chaudret, B.; van Leeuwen, P. W. N. M., Soluble Platinum Nanoparticles Ligated by Long-Chain N-Heterocyclic Carbenes as Catalysts. *Chem. - Eur. J.* **2017,** 23, 12779-12786. 10.1002/chem.201702288.
42. Cao, Z.; Kim, D.; Hong, D.; Yu, Y.; Xu, J.; Lin, S.; Wen, X.; Nichols, E. M.; Jeong, K.; Reimer, J. A.; Yang, P.; Chang, C. J., A Molecular Surface Functionalization Approach to Tuning Nanoparticle Electrocatalysts for Carbon Dioxide Reduction. *J. Am. Chem. Soc.* **2016,** 138, 8120-8125. 10.1021/jacs.6b02878.
43. Wang, Y.; Wan, X.-K.; Ren, L.; Su, H.; Li, G.; Malola, S.; Lin, S.; Tang, Z.; Hakkinen, H.; Teo, B. K.; Wang, Q.-M.; Zheng, N., Atomically precise alkynyl-protected metal nanoclusters as a model catalyst: observation of promoting effect of surface ligands on catalysis by metal nanoparticles. *J. Am. Chem. Soc.* **2016,** 138, 3278-3281. 10.1021/jacs.5b12730.
44. Udumula, V.; Tyler, J. H.; Davis, D. A.; Wang, H.; Linford, M. R.; Minson, P. S.; Michaelis, D. J., Dual Optimization Approach to Bimetallic Nanoparticle Catalysis: Impact of M1/M2 Ratio and Supporting Polymer Structure on Reactivity. *ACS Catal.* **2015,** 5, 3457-3462. 10.1021/acscatal.5b00830.
45. Chen, G.; Xu, C.; Huang, X.; Ye, J.; Gu, L.; Li, G.; Tang, Z.; Wu, B.; Yang, H.; Zhao, Z.; Zhou, Z.; Fu, G.; Zheng, N., Interfacial electronic effects control the reaction selectivity of platinum catalysts. *Nat. Mater.* **2016,** 15, 564-569. 10.1038/nmat4555.
46. Pan, C.; Pelzer, K.; Philippot, K.; Chaudret, B.; Dassenoy, F.; Lecante, P.; Casanove, M.-J., Ligand-Stabilized Ruthenium Nanoparticles: Synthesis, Organization, and Dynamics. *J. Am. Chem. Soc.* **2001,** 123, 7584-7593. 10.1021/ja003961m.
47. Lara, P.; Rivada-Wheelaghan, O.; Conejero, S.; Poteau, R.; Philippot, K.; Chaudret, B., Ruthenium Nanoparticles Stabilized by N-Heterocyclic Carbenes: Ligand Location and Influence on Reactivity. *Angew. Chem., Int. Ed.* **2011,** 50, 12080-12084. 10.1002/anie.201106348.
48. Cui, X.; Zhang, Y.; Shi, F.; Deng, Y., Ruthenium-catalyzed nitro and nitrile compounds coupling with alcohols: alternative route for N-substituted amine Synthesis. *Chem. Eur. J.* **2011,** 17, 2587-2591. 10.1002/chem.201003095.
49. Corma, A.; Concepcion, P.; Serna, P., A different reaction pathway for the reduction of aromatic nitro compounds on gold catalysts. *Angew. Chem., Int. Ed.* **2007,** 46, 7266-7269. 10.1002/anie.200700823.
50. Gelder, E. A.; Jackson, S. D.; Lok, C. M., The hydrogenation of nitrobenzene to aniline: a new mechanism. *Chem. Commun.* **2005**, 522-524. 10.1039/b411603h.
51. Mahata, A.; Rai, R. K.; Choudhuri, I.; Singh, S. K.; Pathak, B., Direct vs. indirect pathway for nitrobenzene reduction reaction on a Ni catalyst surface: a density functional study. *Phys. Chem. Chem. Phys.* **2014,** 16, 26365-26374. 10.1039/c4cp04355c.
52. Zhang, L.; Jiang, J.; Shi, W.; Xia, S.; Ni, Z.; Xiao, X., Insights into the hydrogenation mechanism of nitrobenzene to aniline on Pd_3/Pt(III): a density functional theory study. *RSC Adv.* **2015,** 5, 34319-34326. 10.1039/c5ra02389k.
53. Tomkins, P.; Gebauer-Henke, E.; Leitner, W.; Mueller, T. E., Concurrent Hydrogenation of Aromatic and Nitro Groups over Carbon-Supported Ruthenium Catalysts. *ACS Catal.* **2015,** 5, 203-209. 10.1021/cs501122h.

54. Greenfield, H., Hydrogenation of aniline to cyclohexylamine with platinum metal catalysts. *J. Org. Chem.* **1964,** 29, 3082-4. 10.1021/jo01033a512.
55. Chatterjee, M.; Sato, M.; Kawanami, H.; Ishizaka, T.; Yokoyama, T.; Suzuki, T., Hydrogenation of aniline to cyclohexylamine in supercritical carbon dioxide: Significance of phase behaviour. *Appl. Catal., A* **2011,** 396, 186-193. 10.1016/j.apcata.2011.02.016.
56. Rubio-Marques, P.; Leyva-Perez, A.; Corma, A., A bifunctional palladium/acid solid catalyst performs the direct synthesis of cyclohexylanilines and dicyclohexylamines from nitrobenzenes. *Chem. Commun.* **2013,** 49, 8160-8162. 10.1039/c3cc44064h.
57. Oh, S. G.; Mishra, V.; Cho, J. K.; Kim, B.-J.; Kim, H. S.; Suh, Y.-W.; Lee, H.; Park, H. S.; Kim, Y. J., One pot catalytic NO2 reduction, ring hydrogenation, and N-alkylation from nitroarenes to generate alicyclic amines using Ru/C-NaNO2. *Catal. Commun.* **2014,** 43, 79-83. 10.1016/j.catcom.2013.09.012.
58. Mishra, V.; Cho, J. K.; Shin, S.-H.; Suh, Y.-W.; Kim, H. S.; Kim, Y. J., Ruthenium-Na2CO3-catalyzed one-pot synthesis of ring-hydrogenated carbamates from aromatic amines and organic carbonates under H2. *Appl. Catal., A* **2014,** 487, 82-90. 10.1016/j.apcata.2014.09.013.
59. Makaryan, I. A.; Savchenko, V. I., N-Arylhydroxylamines transformation in the presence of heterogeneous catalysts. *Stud. Surf. Sci. Catal.* **1993,** 75, 2439-42.
60. Sheldon, R. A.; van Bekkum, H.; Editors, *Fine Chemicals through Heterogeneous Catalysis*. Wiley-VCH Verlag GmbH: 2001; p 611 pp.
61. Blaser, H.-U., A Golden Boost to an Old Reaction. *Science* **2006,** 313, 312-313. 10.1126/science.1131574.
62. Corma, A.; Serna, P., Chemoselective Hydrogenation of Nitro Compounds with Supported Gold Catalysts. *Science* **2006,** 313, 332-334. 10.1126/science.1128383.
63. Solomina, T. A.; Ibrasheva, R. K.; Leonova, G. I.; Mordovin, V. P.; Zhubanov, K. A.; Turganbaev, B. D., Prospects of catalytic reduction of aromatic nitro compounds by hydrogen. *Int. J. Hydrogen Energy* **1995,** 20, 159-61. 10.1016/0360-3199(93)e0013-b.
64. Jafarpour, L.; Stevens, E. D.; Nolan, S. P., A sterically demanding nucleophilic carbene: 1,3-bis(2,6-diisopropylphenyl)imidazol-2-ylidene. Thermochemistry and catalytic application in olefin metathesis. *J. Organomet. Chem.* **2000,** 606, 49-54. 10.1016/s0022-328x(00)00260-6.
65. Kresse, G.; Furthmüller, J., Efficiency of ab-initio total energy calculations for metals and semiconductors using a plane-wave basis set. *Comput. Mater. Sci.* **1996,** 6 (1), 15-50. 10.1016/0927-0256(96)00008-0.
66. Kresse, G.; Hafner, J., Ab initio molecular dynamics for liquid metals. *Phys. Rev. B* **1993,** 47 (1), 558-561.
67. Kresse, G.; Furthmüller, J., Efficient iterative schemes for *ab initio* total-energy calculations using a plane-wave basis set. *Phys. Rev. B* **1996,** 54 (16), 11169-11186.
68. Kresse, G.; Hafner, J., *Ab initio* molecular-dynamics simulation of the liquid-meta-amorphous-semiconductor transition in germanium. *Phys. Rev. B* **1994,** 49 (20), 14251-14269.
69. Blöchl, P. E., Projector augmented-wave method. *Phys. Rev. B* **1994,** 50 (24), 17953-17979.
70. Kresse, G.; Joubert, D., From ultrasoft pseudopotentials to the projector augmented-wave method. *Phys. Rev. B* **1999,** 59 (3), 1758-1775.
71. Perdew, J. P.; Burke, K.; Ernzerhof, M., Generalized Gradient Approximation Made Simple. *Phys. Rev. Lett.* **1996,** 77 (18), 3865-3868.
72. Momma, K.; Izumi, F., VESTA 3 for three-dimensional visualization of crystal, volumetric and morphology data. *J. Appl. Crystallogr.* **2011,** 44 (6), 1272-1276. doi:10.1107/S0021889811038970.
73. Tang, W.; Sanville, E.; Henkelman, G., A grid-based Bader analysis algorithm without lattice bias. *J. Phys.: Condens. Matter* **2009,** 21, 084204/1-084204/7. 10.1088/0953-8984/21/8/084204.
74. Fishman, M.; Zhuang, H. L.; Mathew, K.; Dirschka, W.; Hennig, R. G., Accuracy of exchange-correlation functionals and effect of solvation on the surface energy of copper. *Phys. Rev. B: Condens. Matter Mater. Phys.* **2013,** 87, 245402/1-245402/7. 10.1103/PhysRevB.87.245402.
75. Mathew, K.; Sundararaman, R.; Letchworth-Weaver, K.; Arias, T. A.; Hennig, R. G., Implicit solvation model for density-functional study of nanocrystal surfaces and reaction pathways. *J. Chem. Phys.* **2014,** 140, 084106/1-084106/8. 10.1063/1.4865107.
76. del Rosal, I.; Truflandier, L.; Poteau, R.; Gerber, I. C., A Density Functional Theory Study of Spectroscopic and Thermodynamic Properties of Surfacic Hydrides on Ru (0001) Model Surface: The Influence of the Coordination Modes and the Coverage. *J. Phys. Chem. C* **2011,** 115, 2169-2178. 10.1021/jp110090e.

Table of contents